Astron. Astrophys. 331, 262–270 (1998)

ASTRONOMY AND ASTROPHYSICS

A new ROSAT discovered polar near the lower period limit: RX J1015.5+0904 in Leonis⋆

V. Burwitz[1], K. Reinsch[1,†], A.D. Schwope[2,†], P.J. Hakala[3], K. Beuermann[1,4], Th. Rousseau[1], H.-C. Thomas[5], B.T. Gänsicke[1], V. Piirola[6], and O. Vilhu[7]

[1] Universitäts-Sternwarte Göttingen, Geismarlandstr. 11, D-37083 Göttingen, Germany
[2] Astrophysikalisches Institut Potsdam, An der Sternwarte 16, D-14482 Potsdam, Germany
[3] Mullard Space Science Laboratory, University College London, Holmbury St Mary, Dorking, Surrey RH5 6NT, UK
[4] MPI für Extraterrestrische Physik, Giessenbachstr. 1, D-85740 Garching, Germany
[5] MPI für Astrophysik, Karl-Schwarzschild-Str. 1, D-85740 Garching, Germany
[6] Tuorla Observatory, FIN-21500 Piikkio, Finland
[7] Observatory and Astrophysics Laboratory, Box 14, FIN-00014 Helsinki, Finland

Received 28 August 1997 / Accepted 24 October 1997

Abstract. We have identified the bright, soft, X-ray source RX J1015.6+0904 detected during the ROSAT All-Sky Survey with a new AM Herculis binary (polar). Its soft X-ray light curve is typical for a system with a one-pole accretion geometry and shows a bright phase lasting about 0.75 of the binary orbit with ROSAT PSPC countrates of up to 10 cts/s. The bright phase is interrupted by a 3 min long dip with zero countrate where the X-ray emission from the accretion region must be absorbed by the accretion stream crossing our line-of-sight. From the X-ray dip times we derive an orbital period P_{orb} = 79.87946(7) min making this system another member of the new group of polars discovered near the theoretical lower period limit for magnetic CVs. In the optical, the light curve is double-humped and the system varies between V = 16-17 mag in the high state. The optical light is highly polarized with the degree of circular polarization varying between -5% and +30% in R and -5% and 22% in I which is a strong indication for the magnetic nature of the system. The shape of the optical light curve and the broad optical continuum component seen as additional light during the bright-phase can be explained by cyclotron emission in a magnetic field of ∼23 MG in the accretion region. At this field strength only the higher cyclotron harmonics are present in the optical and are smeared to an almost featureless continuum at a viewing angle $\theta \sim 55°$. The orbital inclination of the new AM Her binary can be constrained to $50° \lesssim i \lesssim 75°$ and the mass ratio must be $6.3 < Q = M_1/M_2 < 12.5$ where the mass of the secondary star is estimated to $M_2 = 0.09\,M_\odot$. No features of the late M-type secondary are present in our low-state optical spectra, providing a lower limit for the distance to RX J1015.6+0904 of $d > 100$ pc

Key words: accretion, accretion disks – stars: individual (RX J1015.6+0904) – stars: novae, cataclysmic variables – X-rays: stars – polarization

1. Introduction

The ROSAT All-Sky Survey (RASS) and subsequent optical identifications of bright, soft X-ray sources led to the discovery of a significant number of new polars or AM Herculis binaries (see e.g. Beuermann & Burwitz 1995, Beuermann et al. 1995, Schwope 1995, Warner 1995, Beuermann 1997, and references therein). The new systems not only increased the statistics for studies of the bulk class properties (e.g. period, magnetic field strength, and spatial distributions), but also revealed the existence of systems with physical parameters which have hitherto only theoretically been predicted.

One such example are polars with orbital periods below 80 min, i.e. close to the theoretical minimum orbital period where the companion star moves more or less rapidly towards degeneracy (Paczynski & Sienkiewicz 1981, Rappaport et al. 1982, Nelson et al. 1985, and references therein). Evolutionary scenarios (e.g. Kolb & de Kool 1993) have predicted a peak of systems with $P_{\rm orb} \sim 80$ min. The first such systems have only recently been found: EV UMa (= RE 1307+535, Osborne et al. 1994, Hakala et al. 1994), FH UMa (= RX J1047.1+6335, Singh et al. 1995), and RX J0132.7−6554 and RX J2022.6−3954 (Burwitz et al. 1997).

Send offprint requests to: V. Burwitz (burwitz@mpe.mpg.de)

⋆ Based on observations collected at the European Southern Observatory, La Silla, Chile with the 2.2-m telescope of the Max-Planck-Society in MPI time and with various telescopes in ESO time (ESO N^{os} 50.6-021 and 54.D-0698).

† Visiting Astronomer, German-Spanish Astronomical Center, Calar Alto, operated by the Max-Planck-Institute für Astronomie Heidelberg jointly with the Spanish National Commission for Astronomy.

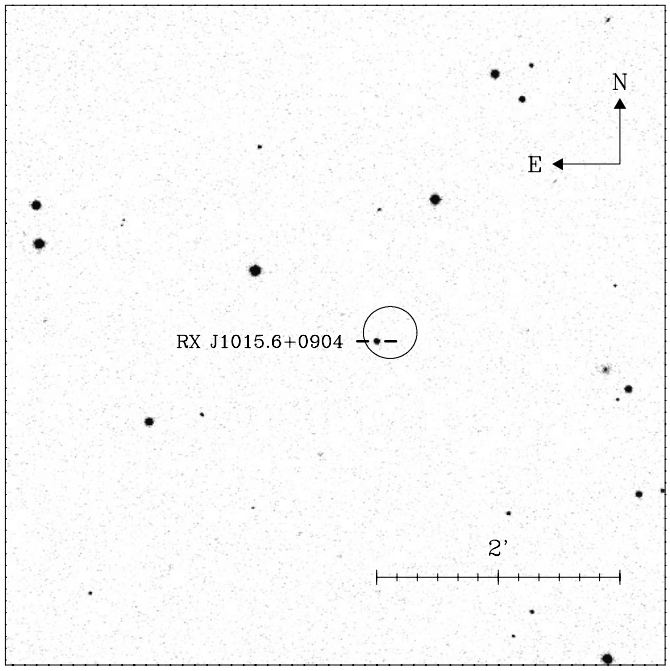

Fig. 1. 30 sec V-filter CCD image obtained with the ESO 2.2-m telescope showing the location of the V∼16.5 mag optical counterpart (α_{2000}= $10^h15^m34\overset{s}{.}7$, δ_{2000} = +09°04′43″) of the RASS X-ray source RX J1015.6+0904. The uncertainty of the RASS X-ray position is given by the 99% confidence (∼ 13″) error circle. More accurate X-ray positions have been obtained from our pointed PSPC and HRI data. The corresponding error circles coincide with the optical position but are too small to be displayed on the scale of this CCD image.

In this paper, we report the discovery of a further short-period AM Herculis system, RX J1015.6+0904 (henceforth 1015+09) and present the analysis of our X-ray data (ROSAT survey and pointed observations) and optical follow-up data (CCD photometry, polarimetry and time-resolved spectroscopy). A preliminary analysis of our optical and X-ray photometry of 1015+09 has been presented in Burwitz et al. (1995).

2. Observations

1015+09 has been discovered during the RASS as a new bright (∼ 1.15 PSPC cts/s) and highly variable soft X-ray source. In subsequent optical observations we have identified 1015+09 as a new polar with a V = 16-17 mag optical counterpart shown in Fig. 1. A summary of our optical CCD photometry, polarimetry, and spectroscopy is given in Table 1.

2.1. CCD photometry

Our photometric observations of 1015+09 were obtained on 3 nights in January/February 1995 at the 0.9-m Dutch telescope at ESO in Chile. For this we used ESO's CCD#33 which is a back illuminated thinned 512×512 pixel^2 Tektronics CCD with 27×27 μm^2 pixels. We obtained further photometry in May 1995 using the AIP 0.7-m telescope in Potsdam, Germany. Here a 1024×1024 pixel^2 Tektronics CCD with 24×24 μm^2 pixels was used.

Table 1. Journal of optical observations.

Date	HJD range (+2440000)	No. exp.	Wavelength range (Å)	Res. (Å)	Int. (s)
CCD photometry					
95/01/31	9748.8391–.8983	29	V		120
95/02/05	9753.8939–.9003	1/1/1	R/V/B		180/120/180
95/02/06	9754.7779–.9002	66	V		120
95/05/04	9842.3810–.4535	20	V		240
Polarimetry					
94/02/04	9387.6130–.6721	30	R		120
94/02/04	9387.6792–.7374	30	I		120
Spectroscopy					
92/01/07	8628.8540	1	3800–9106	24.0	1800
93/02/16	9034.5068–.5979	10	3310–5508	7.0	720
93/02/16	9034.5068–.5979	10	5526–9726	7.7	720
93/02/17	9035.5060–.6103	15	3310–5508	7.0	480
93/02/17	9035.5060–.6103	15	5526–9726	7.7	480
93/02/18	9036.6834	1	3800–9120	24.0	300
93/02/18	9036.6906–.7926	21	3472–5390	5.6	300
93/02/19	9037.7002–.7526	12	3472–5390	5.6	300
95/02/08	9756.6204–.7325	33	4200–5100	1.4	171
95/02/08	9756.6204–.7325	33	7750–8630	1.4	171

From the CCD direct images, differential photometry was derived by integrating the fluxes of the object, nearby comparison stars contained in the field of view, and the sky background using circular apertures. An absolute calibration of the V-filter data was derived from observations of photometric standard stars (Landolt 1992). The color terms for the comparison stars were determined from the B, V, and R images of the field. The stability of the photometry was checked from the standard deviations of the flux differences of the comparison stars.

2.2. Polarimetry

In order to confirm the AM Herculis nature of 1015+09, photopolarimetric data was obtained at the 2.5-m Nordic Optical Telescope (NOT) in February 1994. We used imaging polarizing optics, consisting of a superachromatic quarter-wave retarder plate and a calcite crystal. This optical configuration produces double images of the stars in the field. Circular polarization can then be measured from the ratio of fluxes in these images. The detector used was a front illuminated Tektronix 520×520 pixel^2 chip. All the resulting frames were bias-subtracted and the zero polarization at the position of the source was calibrated using exposures of unpolarized stars at the same position on the chip.

These observations cover a period of three hours. The first half of the observations were carried out in the R band, whilst the remaining half was done in the I band. All the observations had an exposure time of 120 seconds and they were taken as

Table 2. Journal of X-ray observations.

Date	HJD range (+2440000)	No. of OBIs[a]	countrate (cts/s)	HR1	exp. (s)
ROSAT All-Sky Survey					
90/11/15–90/11/16	8210.5977–8212.2657	22	1.15(10)	–0.85(4)	416
ROSAT pointed PSPC data					
93/11/09–93/11/11	9301.4603–9302.9308	7	4.79(3)	–0.87(1)	5185
ROSAT pointed HRI data					
94/05/14–94/05/15	9487.3326–9488.4262	7	0.31(1)		14997

[a] OBI: observation interval

Table 3. Observed times of the centers of the X-ray dips.

HJD (-2400000)	Error (days)	O−C (days)	Epoch (cycles)	Instrument
49302.8587	0.001	0.0000	-3338	PSPC
49487.3580	0.001	-0.0009	-12	HRI
49487.4135	0.001	0.0005	-11	HRI
49488.3565	0.001	-0.0005	6	HRI
49488.4120	0.001	0.0009	7	HRI

an automated exposure series yielding a true time resolution of just under three minutes.

2.3. Spectroscopic observations

The January 1992 discovery spectrum as well as the February 1993 time resolved spectroscopic observations of 1015+09 were obtained at ESO using the ESO/MPI 2.2-m telescope with EFOSC2 equipped with ESO CCD#19 which is a front illuminated 1024×1024 pixel^2 Thompson CCD with 19×19 μm^2 pixels. In February 1993 and February 1995 we also obtained spectra with the MPIA 3.5-m telescope at Calar Alto, Spain using the double beam spectrograph TWIN with a beamsplitter at 5500 Å. During the 1993 run the blue channel was equipped with the RCA#10 1024×640 pixel^2 CCD with 15×15 μm^2 pixels and the red channel with the GEC#14 1155×768 pixel^2 CCD with 22.5×22.5 μm^2 pixels. For the trailed spectra of 1015+09 obtained during the 1995 observing run the blue and red channels were equipped with the TEK#11 and TEK#12 1024×1024 pixel^2 Tektronics CCDs with 24×24 μm^2 pixels, respectively. Slit widths of $1\farcs0$ and $1\farcs5$ were used to adjust to the different seeing conditions during the individual nights.

The long-slit spectroscopic CCD images were reduced using the MIDAS software packages provided by ESO. A flux calibration was obtained from observations of spectrophotometric standard stars (Hamuy et al. 1992, 1994) and is accurate to about 20%. This uncertainty includes possible slit loss errors.

2.4. X-ray

Pointed PSPC and HRI observations of 1015+09 were obtained with ROSAT in addition to the RASS observations. The details of the X-ray observations such as observing dates, exposure times, number of observation intervals, mean countrates and hardness ratios are summarized in Table 2. The hardness ratio HR1 denotes the number of photons above 0.4 keV minus the number of photons below 0.4 keV divided by the total number of photons in the 0.1-2.4 keV ROSAT energy band. We reduced all our X-ray data with the EXSAS software package provided by the MPE Garching (Zimmermann et al. 1994).

3. Results and discussion

3.1. Orbital period, X-ray and optical lightcurves

1015+09 shows strong modulations of the X-ray and optical fluxes repeating about every 80 min which turned out to be the orbital period of the system (cf. Fig. 2**a-g**). In soft X-rays, we see a bright phase lasting $\sim$ 0.75 of the orbital period. During the rest of the orbit (faint phase) the system becomes undetectable probably because the accretion pole disappears behind the limb of the white dwarf. The optical lightcurve is characterized by a double-hump-structured bright phase coinciding with the X-ray bright phase and a flat bottom during the X-ray faint phase. The first hump during the bright phase is brighter than the second. The full amplitude of the optical light curve is $\sim$1.0 mag. The rise from minimum to maximum brightness takes place within only 3 min just as the X-ray bright phase begins. The shape of the optical light curve is typical for polars and can be understood as cyclotron beaming (e.g. Schwope 1995).

The X-ray lightcurve shows a pronounced dip at the center of the bright phase. From a period search using the observed X-ray dip times given in Table 3 we obtain the following ephemeris:

$$T_{\rm dip} = \text{HJD } 2449488.023703(61) + 0.055471850(46) \times E \quad (1)$$

The X-ray dip lasts about 3 min which corresponds to $\Delta\varphi = 0.04$. In the optical there is no sharp dip as in the X-rays even though individual points around phase $\varphi = 0$ lie slightly lower than the optical minimum brightness. However, dips at phase $\varphi = 0$ are present in our circular polarization data.

3.2. Optical photopolarimetry

Given that our photopolarimetric data (cf. Fig. 2**f-i**) are not taken simultaneously at different wavelengths, cover only two colours (R and I), and do not have any linear polarization information, we have not tried to model them in greater detail. However, a qualitative interpretation of the photopolarimetric data in this case is rather straightforward. First of all, our polarimetry confirms that the optical modulation is due to cyclotron emission from one pole and, thus, the system is a single-pole accreting

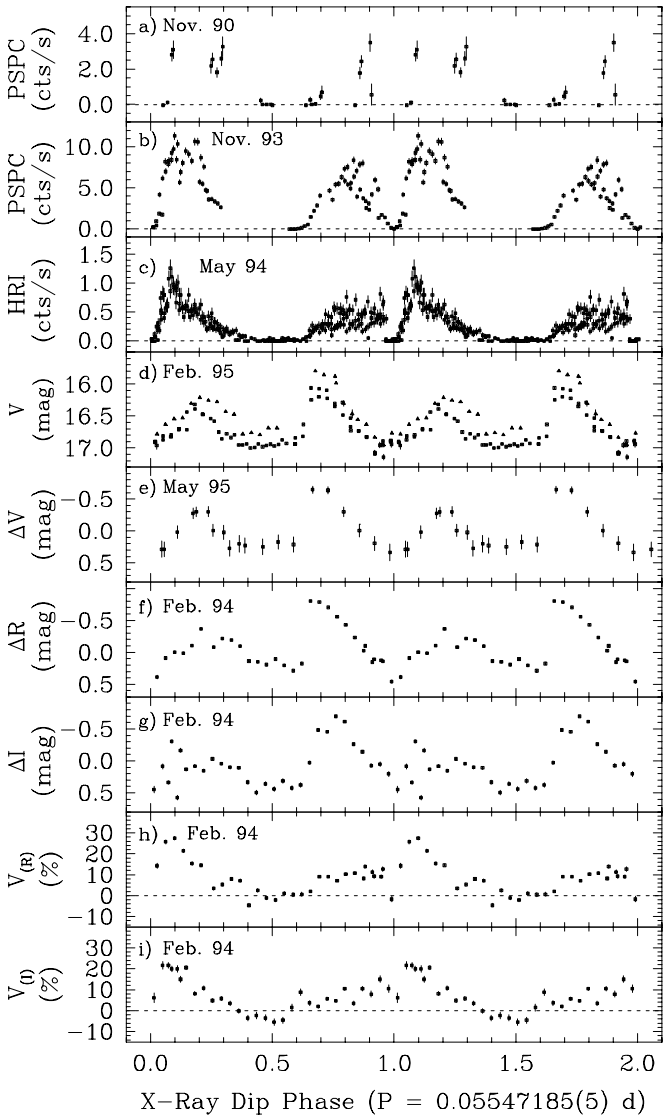

Fig. 2. Summary of X-ray, optical photometric, and polarimetric data: **a** RASS Nov. 1990 X-ray data, **b** Nov. 1993 pointed PSPC X-ray data, **c** May 1994 pointed HRI X-ray data, **d** Jan./ Feb. 1995 V photometry (△: Jan. 31, □: Feb. 06), **e** May 1995 V photometry, **f-g** Feb., 2 1994 R and I photometry and **h-i** the corresponding R and I circular polarimetry. All the data are folded with the orbital period according to the ephemeris given in Eq. 1 and are shown over two cycles for clarity.

polar. Secondly, the asymmetry of the optical light curves suggests that the cyclotron emission region is extended. From the fraction of the orbit where we detect circular polarization (0.75) we can deduce that either the system has a low inclination or the accretion region is located near the white dwarf rotational pole closest to the observer. Inclinations in the range 30°-70° would yield magnetic colatitudes of 68°-27°, respectively (see Cropper 1990 for computing the viewing angle θ versus the inclination, the colatitude, and the phase).

As we only have photopolarimetric data in R and I bands, it is not possible to base an accurate measurement of the white dwarf field strength on our observations. However, the fact that the V, R, and I light curves are almost identical in terms of modulation amplitude and that the R and I polarization curves also agree can give us some clues on the field involved. The systems with white dwarf field strengths above 30 MG typically do not show clear cyclotron modulation in the I band (see for instance HU Aqr (Hakala et al. 1993) and VV Pup (Piirola, Coyne and Reiz, 1990)). The wavelength dependence of the cyclotron emission modulation in 1015+09 resembles that of BY Cam (Piirola et al. 1994), in which case the white dwarf field strength might be in the range 20-30 MG.

3.3. Low-resolution spectroscopy

From our low-resolution optical spectra obtained in Feb. 1993 during a high-state of 1015+09 we have calculated average bright and faint phase spectra (see Fig. 3), with a phase coverage $0.19 < \varphi < 0.34$ and $0.65 < \varphi < 0.92$ for the bright-phase spectrum and $0.42 < \varphi < 0.58$ and $0.93 < \varphi < 1.07$ for the faint-phase spectrum. In order to improve the signal-to-noise of the faint-phase spectrum the faint- and dip-phase intervals were combined as our photometry shows that they both have similar flux levels. The difference between the bright-phase and the faint-phase spectra is basically a smooth continuum with a sharp decline shortwards of $\sim$ 5300 Å and can be explained as the contribution of cyclotron radiation from the accretion region.

We computed cyclotron model spectra using the method described by Rousseau et al. (1996). Given the temperature structure of an atmosphere which is heated by a stream of free falling protons which loose their energy by Coulomb encounters with atmospheric electrons (Woelk & Beuermann, 1993), cyclotron spectra were calculated for a given surface field B as a function of the mass flow rate $\dot{m}$. From a fit to the observed high-state difference spectrum (see Fig. 3**c**) of 1015+09 at wavelengths larger than 4000Å, we determined the viewing angle of the magnetic field lines θ, the magnetic field strength B, and the range of mass flow rates $\dot{m}$ in the accretion spot(s).

It is not possible to fit the spectrum with a single mass flow rate, because single flow rates produce cyclotron humps which are not broad enough to fit to the spectrum. Therefore, the fit requires a range of $\dot{m}$ values. We first used the same range of mass flow rates found by Rousseau et al. (1996) for UZ For ($\sim$ 1 to $\sim 10^{-4}$ g cm^{-2}s^{-1}) represented by one value per decade centered at each decade. This yields a fit (not shown for brevity) which overestimates the weight of the higher mass flow rate (0.3 g cm^{-2}s^{-1}) in order to reproduce the red wing of the spectrum, so that the flux becomes too large at $\sim$ 5300 Å. Furthermore, the values of $\dot{m} < 0.03$ g cm^{-2}s^{-1} do not substantially contribute to the total flux. Thus, only three mass flow rates (0.3, 0.1, 0.03 g cm^{-2}s^{-1} cf. Fig. 3**c**) are necessary to fit the observed cyclotron spectrum. They yield a much better fit for all possible values of the remaining parameters θ and B.

The best fit to the cyclotron spectrum yields $\theta = 55° \pm 10°$ and $B = 23 \pm 3$ MG. For larger angles, the theoretical spectrum becomes too structured and there is no value of B which produces the observed smooth continuum. For smaller

angles the fits require larger contributions of small accretion rates which in turn also lead to structured spectra. Lower values of B do not fit to the observed spectrum because the flux is not reproduced at short wavelengths, and higher values of B generate again spectra which are too structured and do not fit to the observed smooth continuum. These values depend only weakly on the mass of the white dwarf which was assumed to be $M_1 = 0.6\,M_\odot$.

The "bombardment solution", for which a strong shock does not develop (Kuijpers & Pringle 1982, Woelk & Beuermann 1992), is valid for the whole $\dot{m}$-range for this value of B. Thus, the temperature structure of the heated atmosphere we used for computing our basic cyclotron spectra is justified *a posteriori*.

No cyclotron features are present in our low-state discovery spectrum of 1015+09 which was taken during an optical low state when the optical flux was about a factor 5 less than during the high state (see Fig. 3**d**). The 30 min integration covers the faint phase and part of the bright phase ($\varphi = 0.23 - 0.61$). Zeeman absorption features of the Balmer lines may be present but the low-state spectrum is too noisy to derive the magnetic field strength from their positions.

The very weak emission lines displayed in the low-state spectrum indicate that accretion had almost ceased at the time of the observations. In that case, the white dwarf is likely to be a significant source of the optical flux (e.g. Schmidt et al. 1981). We have tested the possible contribution of the white dwarf to the low-state spectrum using the model spectra of Gänsicke et al. (1995). The observed continuum slope favours a rather cool primary, a model for $T_{\rm wd} = 8000$ K, $M_{\rm wd} = 0.8 M_\odot$ and $d = 100$ pc is shown in Fig. 3**d**. The flux in the blue part of the spectrum may be somewhat depressed by Zeeman absorption and, therefore, white-dwarf temperatures up to 12 000 K cannot be excluded.

Such a low temperature is not unusual for a short period system, even though it is at the low end of observed white dwarf temperatures in polars (Sion 1991). For a more moderate temperature of $T_{\rm wd} = 15\,000$ K, the observed optical flux requires $d \approx 300$ pc. A distance that large would yield unrealistically high accretion rates (cf. sect. 3.7). We conclude that the white dwarf in 1015+09 is likely to have $T_{\rm wd} = 8000 - 12\,000$ K.

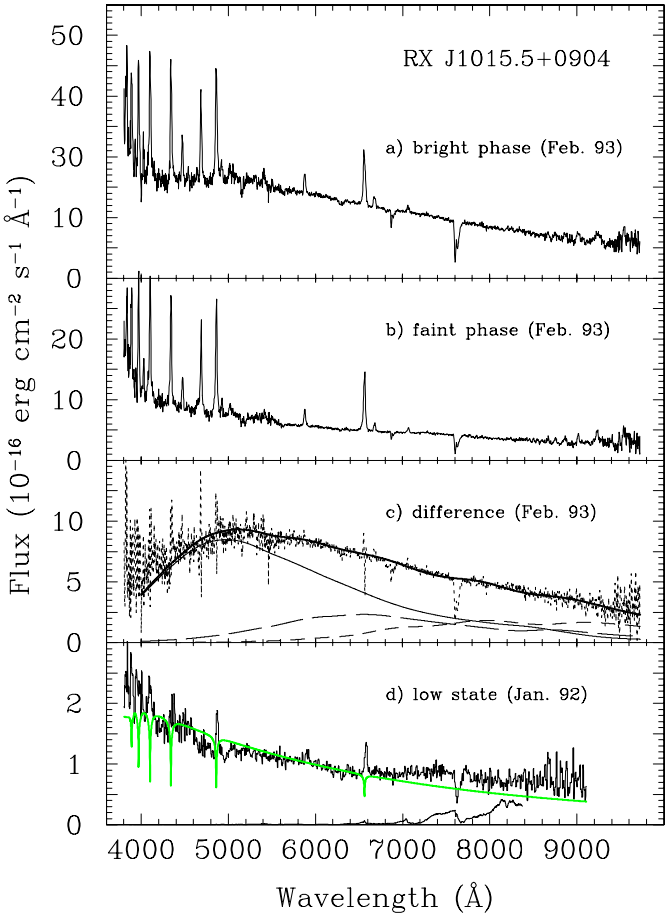

Fig. 3. Optical spectra of 1015+09. **a** and **b** Average bright and faint phase spectra of 1015+09 obtained during a high-state in February 1993. **c** Difference spectrum of **a** and **b** (dotted line), cyclotron model spectrum for $B = 23$ MG and $\theta = 55°$ (thick solid line), and the contributions of the individual mass flow rates: $\dot{m} = 0.3$ g cm^{-2}s^{-1} (thin solid line), $\dot{m} = 0.1$ g cm^{-2}s^{-1} (long dashed line), and $\dot{m} = 0.03$ g cm^{-2}s^{-1} (short dashed line). **d** Low-resolution discovery spectrum taken in January 1992 during a low-state. The overlying model spectrum (grey line) shows the possible contribution of the white-dwarf photosphere ($T_{\rm wd} = 8000$ K, $M_{\rm wd} = 0.8 M_\odot$, $d = 100$ pc). Additionally, the spectrum of the late-type M-star VB 8 scaled down by a factor of 700 is shown. The spectral features do not match the remaining flux distribution in the red and, therefore, the secondary in 1015+09 can contribute at most 10% in the R band.

3.4. Distance estimate

The flux remaining in the red part of the low-state optical spectrum of 1015+09 after subtraction of the possible white-dwarf contribution does not show the spectral features expected for a late-type M dwarf secondary (cf. Fig. 3**d**). This flux may be cyclotron emission from low mass-flow rates ($\dot{m} \lesssim 0.01$ g cm^{-2} s^{-1}). The contribution of the secondary star to the total flux in the R band can be about 10% at most. So, the method described by Bailey (1981) can be adapted to derive a lower limit for the distance of 1015+09. A Roche-lobe filling red dwarf with an orbital period of 1.3 hours is likely to have a radius of $\sim$0.13 $R_\odot$ and a mass of $\sim$0.1 $M_\odot$ (depending only weakly on $M_1 \sim 0.6 - 1.4 M_\odot$).

A single M-dwarf with similar mass has a spectral type later than M5 such as VB 8 which has infrared colours V$-$K = 7.92 and R$-$K = 5.83 (Reid & Gilmore 1984). Using the improved surface brightness relationship for M dwarfs (Ramseyer 1994) and V$-$K of VB 8, we obtain a K surface brightness S_K=5.44 for the secondary in 1015+09. With R$-$K of VB 8 and R > 20.8 from the Jan. 1992 low-state spectrum of 1015+09, this leads to a lower limit $d > 100$ pc for the distance of 1015+09.

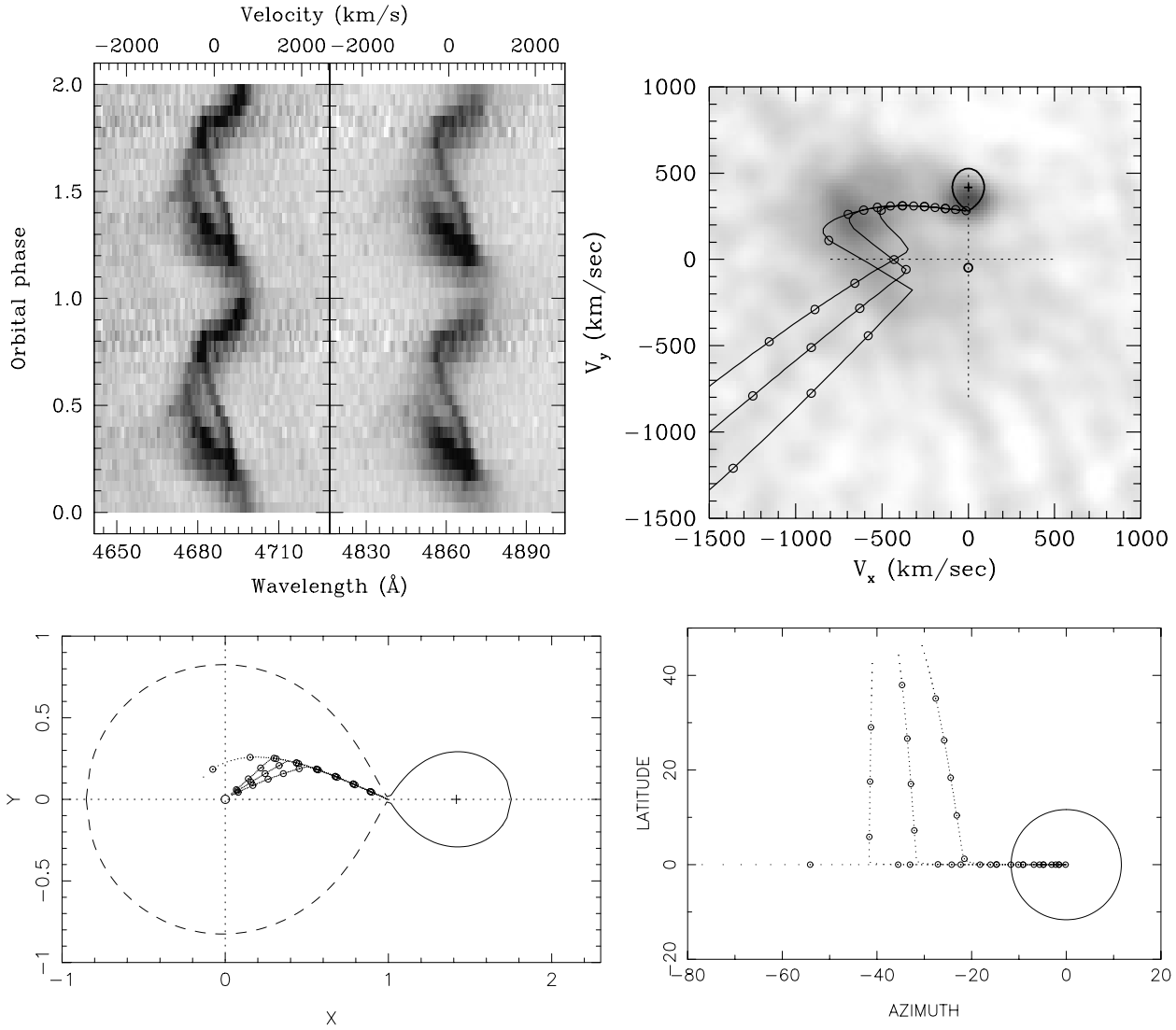

Fig. 4. a *top left panel)* Trailed spectrograms of the He II λ4686 and Hβ emission lines of 1015+09 obtained in Feb. 1995. Phase zero is defined by the center of the X-ray dip. **b** *(top right)* Doppler map of He II λ4686 computed by filtered backprojection of the spectrogram data shown above. The overlay shows the shape of the secondary star, the ballistic and the magnetically controlled part of the stream for a geometry as sketched in the panel below and explained in more detail in the text. The phase shift $\varphi_0 = 0.085$ between the X-ray dip and the blue-to-red zero crossing was taken into account. **c** *(bottom left)* Sketch of the accretion geometry as seen from above the orbital plane. **d** *(bottom right)* Sketch of the accretion geometry as seen by a hypothetic observer on the white dwarf. Shown are the circularly approximated shape of the secondary star, the ballistic stream and three magnetically controlled trajectories leaving the orbital plane. These as well as the spacing of the large symbols correspond to those shown as overlay over the tomogram in panels **b** and **c**.

3.5. Analysis of the high resolution spectrograms

The results of our high-resolution spectral observations described in Sect. 2.3 are shown as a trailed spectrogram of the He II λ4686 and Hβ lines in Fig. 4 (top left panel). For representation in the figure and further analysis we use spectra normalized to a smooth continuum. These were computed by dividing the original spectra by a low-order polynomial fit to regions free of spectral lines. The lines in the trailed spectrogram show the typical characteristics of AM Herculis binaries, they consist of at least two components: The first is a narrow component with a comparatively low radial velocity amplitude which is usually associated with the illuminated hemisphere of the secondary star, and the second is an underlying broad component with higher radial velocity amplitude which originates from the accretion stream. This general pattern can be recognized in all spectral lines in our observation window.

We focus our attention in the following on the line of ionized Helium He II λ4686, which shows the sharpest features. For the further analysis of the line profiles as a function of orbital phase we follow the scheme outlined recently by Schwope et al. (1997) for the case of HU Aqr by first fitting Gaussians to the profile,

thus separating components originating from the stream and the secondary star, followed by a tomogram analysis.

For the line profile fitting we used two or three Gaussians of different width. A least-squares fit to the positions of the narrow emission line component assuming a circular orbit, $v = \gamma + K_2' \sin(i) \sin(2\pi(\varphi - \varphi_0))$, yielded $\gamma = 118 \pm 5\,\mathrm{km\,s^{-1}}$, $K_2' \sin(i) = 329 \pm 6\,\mathrm{km\,s^{-1}}$ and a blue-to-red zero crossing phase $\varphi_0 = 0.085 \pm 0.003$ (where $\varphi = 0$ is defined by the center of the X-ray dip). As in other AM Herculis binaries we attribute the narrow line component to the illuminated hemisphere of the secondary star. Hence, φ_0 is regarded as the phase of inferior conjunction of the secondary star. The systemic velocity γ of nearly $120\,\mathrm{km\,s^{-1}}$ is surprisingly large and is regarded as true systemic velocity of the binary system. Fits with γ fixed at low velocities clearly do not fit our radial velocity data.

The radial velocity amplitude of the photocenter $K_2' \sin(i)$ gives some constraints on the likely inclination i and mass ratio $Q = M_1/M_2$. This has been demonstrated in several previous papers (e.g. Beuermann & Thomas 1990, Schwope et al. 1993, Schwope et al. 1997) where a relation between the radial velocity of the photocenter of a line and the radial velocity of the center of mass has been established. The mass of the secondary star in 1015+09 is estimated using the $(M - R)$ relation for late-type stars given by Neece (1984), $M_2 = 0.09\,\mathrm{M_\odot}$ (very weakly dependent on the mass ratio Q). The absence of eclipses by the secondary star yields an upper limit for the inclination of $i < 75°$, the presence of absorption dips in the X-ray light curves on the other hand limits the inclination to about $i > 50°$. The limits for the orbital inclination and the radial velocity amplitude of the secondary star confine the mass ratio within the range $6.3 < Q < 12.5$. If we assume an intermediate value for the inclination of $i = 60°$, the mass ratio is $Q = 8.7$ and the white dwarf mass $M_1 = 0.79\,\mathrm{M_\odot}$ (orbital velocities of the stars $K_1 = 55\,\mathrm{km\,s^{-1}}$ and $K_2 = 480\,\mathrm{km\,s^{-1}}$). If we assume instead a standard white dwarf with $M_1 = 0.6\,\mathrm{M_\odot}$, the likely mass ratio is $Q = 6.6$ and the orbital inclination is at the upper limit of $i \simeq 75°$ ($K_1 = 65\,\mathrm{km\,s^{-1}}$, $K_2 = 429\,\mathrm{km\,s^{-1}}$).

Further constraints on the mass ratio and the inclination could have been derived if the Na I $\lambda\lambda$ 8183,8194 absorption lines expected from the secondary were detected in our high-resolution spectroscopy in the red. Due to the small flux contribution of the secondary (see section 3.4), however, this was not the case.

3.6. Doppler tomography

A Doppler map of the He II λ4686 emission was computed using the filtered backprojection algorithm developed by Marsh & Horne (1988) (Fig. 4, top right panel). The systemic velocity $\gamma = 118\,\mathrm{km\,s^{-1}}$ was subtracted before backprojection. The map shows mainly two structures, one centered at the likely position of the secondary star on the axis $v_x = 0\,\mathrm{km\,s^{-1}}$, and a second more extended roughly centered at $v_x = -700\,\mathrm{km\,s^{-1}}$, $v_y = 250\,\mathrm{km\,s^{-1}}$. Emission at high velocities $|v| > 1000\,\mathrm{km\,s^{-1}}$ is regarded as spurious and caused by our coarse phase resolution. The second, broader structure clearly originates from the accretion stream, the former is the Doppler image of the narrow emission line component. We modelled the likely location of the emission using the scheme outlined in more detail in Schwope et al. (1997). In short, the stream is assumed to follow initially a ballistic trajectory starting at the inner Lagrangian point L_1. It is redirected somewhere between the two stars by the magnetic field, which is assumed to be dipolar. At each point along the trajectory the velocity components (v_x, v_y) are computed and plotted as an overlay on the Doppler map. In addition, the shape of the secondary star is computed for the given velocities K_1, K_2. Constraints on that procedure are given by the likely mass ratio, the inclination, the phase of the X-ray absorption dip and the magnetic field geometry.

For the model shown in Fig. 4 we used $Q = 8.7$, $i = 60°$, $K_1 \sin i = 48\,\mathrm{km\,s^{-1}}$, $K_2 \sin i = 416\,\mathrm{km\,s^{-1}}$, a colatitude and an azimuth of the magnetic axis of $\beta = 25°$ and $\psi = 40°$, respectively. The latter quantity is the angle spanned by the projection of the magnetic axis onto the orbital plane and the line connecting both stars and is measured in reversed direction with respect to the orbital motion. Using this choice of parameters the stream crosses our line-of-sight towards the white dwarf at an azimuth of $\sim$30° (see Fig. 4, bottom left panel for a view of the accretion geometry as seen from above the orbital plane and bottom right panel, for the likely geometry as seen by a hypothetical observer on the white dwarf), as required to explain the relative phasing of the X-ray absorption dip and the inferior conjunction of the secondary star. In addition, with this choice of geometry the ballistic trajectory does not extend beyond $v_x \simeq -900\,\mathrm{km\,s^{-1}}$, as derived from the Doppler map. The overlay shows that (1) emission from the secondary star is concentrated on the illuminated frontside of the secondary star and that (2) most of the line emission from the stream comes from the threading region, where the stream is redirected. Although one must be cautious interpreting the Doppler map because equal distances in velocity space (v_x, v_y) do not conform to equal distances in (x, y) it seems to be apparent, that the threading or coupling region is significantly brighter than the ballistic part of the stream or than the high velocity part along dipolar field lines.

Table 4. Summary of spectral fits to the survey and pointed PSPC data of 1015+09. $F_{\rm br}$ and $F_{\rm bb}$ are the unabsorbed fluxes in the 0.1-2.4 keV ROSAT band

$N_{\rm H}$ (10^{20} cm^{-2})	k$T_{\rm br}$ (keV)	k$T_{\rm bb}$ (eV)	$F_{\rm br}$ (10^{-11} erg cm^{-2} s^{-1})	$F_{\rm bb}$	χ^2_r	d.o.f.	data set	fit
1.77	20	43.9	0.211	1.22	1.18	11	Nov.90	(**a**)
2.59	20	24.4	0.334	31.10	2.24	70	Nov.93	(**b**)
2.49	20	25.0	0.333	26.83	2.21	71	Nov.93	(**c**)
3.21	20	21.0	0.339	84.53	2.21	71	Nov.93	(**d**)
1.60	20	33.2	0.325	7.21	2.26	71	Nov.93	(**e**)
1.07	20	41.4	0.315	3.73	2.34	71	Nov.93	(**f**)

3.7. X-ray spectra

To analyse the X-ray spectra of 1015+09 we spectrally binned the data in the photon event files so that we have a signal-to-noise

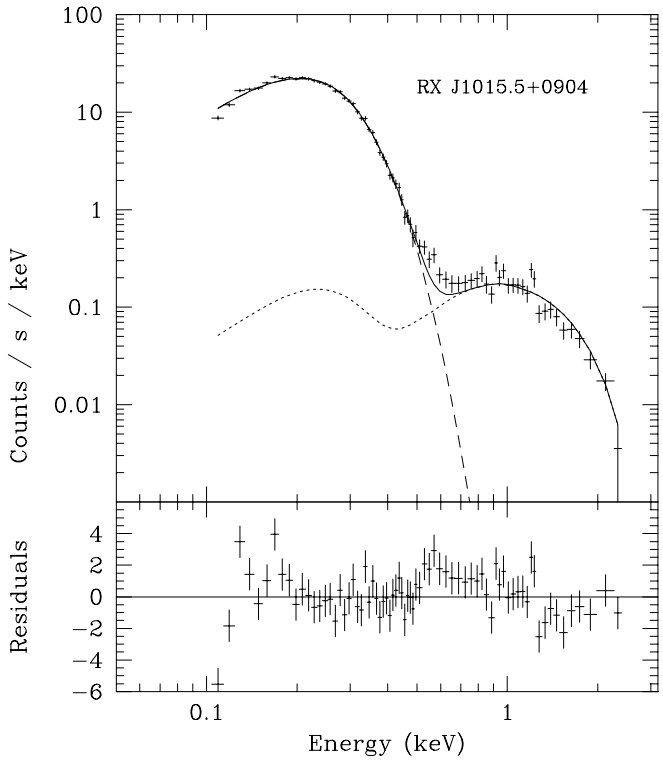

Fig. 5. Best two-component fit (blackbody k$T_{\rm bb}$ = 24.4 eV plus thermal Bremsstrahlung component k$T_{\rm br}$ = 20 keV, $N_{\rm H}$ = 2.59 10^{20} cm^{-2}, see fit **b** in Table 4) to the spectrum of RX J1015.6+0904 derived from the pointed ROSAT PSPC observation.

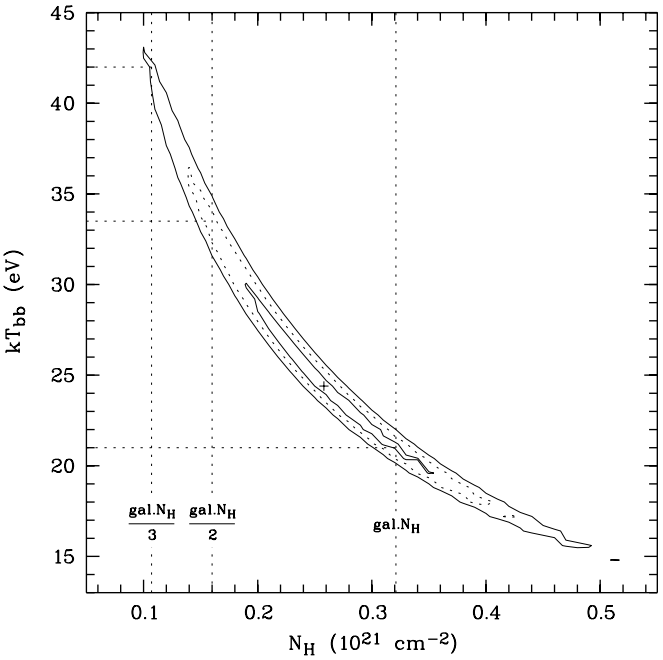

Fig. 6. χ^2-plane spanned by k$T_{\rm bb}$ and $N_{\rm H}$ with k$T_{\rm br}$ fixed at 20 keV. The contours correspond to the 68.33%, 95.45%, and 99.73% confidence levels obtained from fits to the pointed PSPC spectrum shown in Fig. 5. It clearly shows the high correlation between k$T_{\rm bb}$ and $N_{\rm H}$. The values 1/3, 1/2, and full galactic $N_{\rm H}$ are marked by vertical lines. The corresponding k$T_{\rm bb}$ values are indicated by horizontal lines.

ratio of 2 per bin for the RASS data and a signal-to-noise ratio of 5 per bin for the pointed PSPC data (cf. Fig. 5) and fitted them with a model consisting of a blackbody plus a thermal-Bremsstrahlung component.

In order to constrain the temperature range and the neutral hydrogen column density range for the pointed PSPC spectrum we performed a grid search of the χ^2-plane spanned by the blackbody temperature k$T_{\rm bb}$ and the column density $N_{\rm H}$ (cf. Fig. 6) with the thermal-Bremsstrahlung temperature k$T_{\rm br}$ fixed at 20 keV. From this search we obtained the following limits corresponding to the 68% (99%) confidence levels, k$T_{\rm bb}$ = 19-30 (15-43) eV and $N_{\rm H}$ = 0.19-0.35 (0.10-0.52) 10^{21} cm^{-2}. The poor constraints for k$T_{\rm bb}$ and $N_{\rm H}$ are due to the limited energy resolution of the ROSAT PSPC and the strong correlation between k$T_{\rm bb}$ and $N_{\rm H}$.

Keeping k$T_{\rm br}$ = 20 keV fixed, the best fit to the survey data yields $N_{\rm H}$ =1.77 10^{20} cm^{-2} and a fairly high k$T_{\rm bb}$ = 43.9 eV (fit **a** in Table 4). The same type of fit to the pointed PSPC data yields $N_{\rm H}$ =2.59 10^{20} cm^{-2} and k$T_{\rm bb}$ = 24.4 eV (fit **b** in Table 4). Holding both k$T_{\rm br}$ = 20 keV and k$T_{\rm bb}$ = 25 eV fixed we obtain $N_{\rm H}$ =2.49 10^{20} cm^{-2} and a flux ratio $F_{\rm br}/F_{\rm bb}$ = 0.012(1) (fit **c** in Table 4).

In the direction of 1015+09 the full galactic column density obtained from Dickey and Lockman (1990) as implemented in the EXSAS software package is $N_{\rm H,gal}$ = 3.21 10^{20} cm^{-2}. Fig. 6 shows that at least 1/3 of the galactic column density is required to model the X-ray spectrum of 1015+09. Such a value of $N_{\rm H}$ is plausible given the distance of at least 100 pc. Fits (d), (e), and (f) in Table 4 were performed using $N_{\rm H}$ fixed at 1/3, 1/2, and full galactic column density, respectively, and k$T_{\rm br}$ fixed at 20 keV.

The full galactic $N_{\rm H}$ would require a distance of at least 300 pc. At this distance the accretion rate obtained from the total integrated flux $F_{\rm bb} + F_{\rm br}$ would be $\dot{M}_{\rm br+bb} \sim$ 2 10^{17} g s^{-1} which is unusually high for a short-period polar. More plausible values in the range $\dot{M}_{\rm br+bb} \sim$ 4 − 8 10^{14} $(d/100\,{\rm pc})^2$ g s^{-1} are obtained from the fits with 1/3$N_{\rm H\,,gal}$ to 1/2$N_{\rm H\,,gal}$.

4. Conclusions

From our X-ray and optical follow-up observations we can confine the principal physical parameters of the new polar RX J1015.6+0904. The presence of absorption dips in the X-ray light curves implies that the orbital inclination i must be larger than the co-latitude δ of the accretion spot. As the accretion spot completely disappears behind the white dwarf for $\sim$0.25 of the orbit we further have to assume 95° $\lesssim i+\delta \lesssim$ 100°, depending only slightly on i and δ themselves. A somewhat larger value of $i + \delta$ is required for an extended accretion region. In addition, the inclination of the orbital plane is limited by the absence of eclipses by the secondary star to $i \lesssim$ 75°. Taking

these three constraints together we find $50^\circ \lesssim i \lesssim 75^\circ$ and $50^\circ \gtrsim \delta \gtrsim 20^\circ$.

The optical bright phase shows a double-humped structure and coincides with the X-ray bright phase. This is typical for polars with accretion onto one pole and can be understood as cyclotron beaming. An analysis of our featureless cyclotron spectra yields a magnetic field strength $B = 23 \pm 3$ MG and an average viewing angle of the field lines $\theta = 55^\circ \pm 10^\circ$. This value for the field strength is in good agreement with the limits $20\,\mathrm{MG} < B < 30\,\mathrm{MG}$ obtained from our polarimetry. As our average bright-phase spectrum covers $\sim 0.35\,P_{\rm orb}$ the observed cyclotron spectrum includes a more or less wide range of θ, depending on i and δ. The effective θ of our observations lies between $\theta \sim 55^\circ$ and $\theta \sim 70^\circ$ for $i = 50^\circ$, $\delta = 50^\circ$ and $i = 75^\circ$, $\delta = 20^\circ$, respectively. Thus our cyclotron model fits and the large amplitude of the cyclotron beaming indicate that the orbital inclination is probably in the range $50^\circ < i < 60^\circ$. This would imply a comparably large white dwarf mass, $0.8\,\mathrm{M}_\odot \lesssim M_1 \lesssim 1.2\,\mathrm{M}_\odot$.

The accretion region in 1015+09 is clearly structured in the sense that the mass flow rates $\dot{m} \gtrsim 0.1\,\mathrm{g\,cm^{-2}\,s^{-1}}$ contribute $\sim 75\%$ to the total accretion rate from $\sim 30\%$ of the area of the accretion region. Correspondingly, mass flow rates $\dot{m} < 0.1\,\mathrm{g\,cm^{-2}\,s^{-1}}$ contribute only $\sim 25\%$ to the total accretion rate from $\sim 70\%$ of the area of the accretion region. A similar finding was obtained for UZ For (Rousseau et al. 1996). The integrated accretion rate obtained from the fits to the cyclotron emission is $\dot{M}_{\rm cyc} \simeq 4\,10^{13}\,(d/100\,\mathrm{pc})^2\,\mathrm{g\,s^{-1}}$ with a covering factor $f \simeq 2\,10^{-4}\,(d/100\,\mathrm{pc})^2$. The finding that $\dot{M}_{\rm cyc} \ll \dot{M}_{\rm br+bb}$ indicates that mass flow rates $\dot{m} \gg 0.3\,\mathrm{g\,cm^{-2}\,s^{-1}}$ occur which do not contribute to the cyclotron spectrum but lead to soft X-ray emission from the accretion-heated white-dwarf atmosphere.

With a period of 79.879 min RX J1015.6+0904 is a further member of the new group of systems with orbital periods below 80 min formed by the shortest period polars RX J0132.7−6554 and RX J2022.6−3954 ($P_{\rm orb}$ = 77.83 min, $P_{\rm orb}$ = 78.02 min, Burwitz et al. 1997), EV UMa (= RE 1307+535, $P_{\rm orb}$ = 79.69 min, Osborne et al. 1994, Hakala et al. 1994), and FH UMa (= RX J1047.1+6335, $P_{\rm orb} \simeq 80$ min, Singh et al. 1995). Prior to the ROSAT soft X-ray and the WFC EUV surveys, EF Eri ($P_{\rm orb}$ = 81.02 min, Warner 1995) has been the only system at the short-end of the period distribution (Ritter & Kolb 1992). The existence of a peak of systems with $P_{\rm orb} \sim 80$ min has been predicted by evolutionary scenarios (e.g. Kolb & de Kool 1993). The rather low white-dwarf temperature indicated by our low-state spectrum is consistent with evolutionary scenarios predicting that short-period CVs are likely to be rather old systems.

Acknowledgements. We thank the ROSAT team for its enduring work which resulted in the All-Sky-Survey data base and the staff at the La Silla, Calar Alto, and La Palma observatories for their competent assistance during our observing runs. We also thank D.C. Hannikainen, S. Mengel, P. Notni, and A. van Teeseling for their contribution to the observations. This work was supported by the DARA under grants 50 OR 9210 5 and 50 OR 9403 5 and by the Deutsche Forschungsgemeinschaft under grants Re 1100/3-1 and Schw 536/3-1.

References

Bailey J., 1981, MNRAS, 197, 31
Beuermann K., 1997, Perspectives of high-energy astronomy & astrophysics, Agrawal P. (ed.), Tata Inst. of Fund. Res., in press
Beuermann K., Burwitz V., 1995, ASP Conf. Ser. 85, 99
Beuermann K., Burwitz V., Reinsch K., Schwope A.D., Thomas H.-C., 1995, Proc. Abano-Padova Conference on Cataclysmic Variables, Bianchini A., Dellavalle M., Orio M. (eds.), Kluwer, 381
Beuermann K., Thomas H.-C., 1990, A&A 230, 326
Burwitz V., Reinsch K., Schwope A.D., Beuermann K., Mengel S., Notni P., van Teeseling A., Thomas H.-C., 1995, Astron. Ges. Abstract Series 11, 148
Burwitz V., Reinsch K., Beuermann K., Thomas H.-C., 1997, A&A 327, 183
Cropper M., 1990, Space Sci. Rev. 54, 195
Dickey J.M., Lockman F.J., 1990, ARA&A 28, 215
Gänsicke B.T., Beuermann K., de Martino D., 1995, A&A 303, 127
Hakala P. J., Piirola V., Vilhu O., Osborne J. P., Hannikainen D. C., 1994, MNRAS, 271, L41
Hakala P.J., Watson M.G., Vilhu O., Hassall B.J.M., Kellett B.J., Mason K.O. and Piirola V., 1993, MNRAS 263, 61.
Hamuy M., Walker A.R., Suntzeff N.B., 1992, PASP 104, 533
Hamuy M., Suntzeff N.B., Heathcote S.R., 1994, PASP 106, 566
Kolb U., de Kool M., 1993, A&A, 279, L5
Kuijpers J., Pringle J.E., 1982, A&A 114, L4
Landolt A.U., 1992, AJ 104, 340
Marsh T.R., Horne K., 1988, MNRAS 235, 269
Neece G.D., 1984, ApJ 277, 738
Nelson L.A., Chau W.Y., Rosenblum A., 1985, ApJ 299, 658
Osborne J.P., Beardmore A.P., Wheatley P.J., Hakala P., Watson M.G., Mason K.O., Hassall B.J.M., King A.R., 1994, MNRAS 270, 650
Piirola V., Coyne G.V, Reiz A., 1990, A&A 235, 245.
Piirola V., Coyne G.V., Takalo L., Larsson S., Vilhu O., 1994, A&A, 283, 163.
Paczynski B, Sienkiewicz R., 1981, ApJ 248, L101
Ramseyer T.F., 1994, ApJ 425, 243
Rappaport S., Joss P.C., Webbink R.F., 1982, ApJ 254, 616
Reid N., Gilmore G. 1984, MNRAS 206, 19
Ritter H., Kolb U., 1992, A&A 259, 159
Rousseau Th., Fischer A., Beuermann K., Woelk U., 1996, A&A 310, 526
Schmidt G.D., Stockman H.S., Margon B., 1981, ApJ 243, L15
Schwope A.D., 1995, Rev. Modern Astron. 8, 125
Schwope A.D., Beuermann K., Jordan S., Thomas H.-C., 1993, A&A 278, 498
Schwope A.D., Mantel K.-H., Horne K., 1997, A&A 319, 894
Sion E.M., 1991, AJ 102, 295
Singh K.P., Szkody P., Barrett P., et al., 1995, ApJ 453, 95
Warner B., 1995, Cataclysmic Variable Stars, Cambridge University Press
Woelk U., Beuermann K., 1992, A&A 256, 498
Woelk U., Beuermann K., 1993, A&A 280, 169
Zimmermann H.U., Belloni T., Izzo C., Kahabka P., Schwentker O., 1994, MPE Report 257

This article was processed by the author using Springer-Verlag LaTeX A&A style file *L-AA* version 3.